

Thermal attenuation in atom-surface scattering: The multiphonon contribution

G. Armand

*Service de Physique des Atomes et des Surfaces, Département de Physique Générale,
Centre d'Etudes Nucléaires de Saclay, 91191 Gif-sur-Yvette, Cédex, France*

J. R. Manson

Department of Physics and Astronomy, Clemson University, Clemson, South Carolina 29634

C. S. Jayanthi*

*Service de Physique des Atomes et des Surfaces, Département de Physique Générale,
Centre d'Etudes Nucléaires de Saclay, 91191 Gif-sur-Yvette, Cédex, France*

(Received 20 June 1986)

A resummation procedure is presented which allows one to include the contribution of virtual multiphonon exchange in the T -matrix element for the intensity of the specular beam. This procedure uses the exact- T -matrix elements of the one and two virtual-phonon processes as the starting point, quantities which have been calculated previously by the authors. Results are given for the scattering of helium, molecular hydrogen, and neon by the flat (100) face of copper. The intensities yielded by the resummation always lie between those given by the one-phonon and the one-plus-two-phonon processes. It seems that the addition of an even number of phonon events increases the intensity, whereas an odd number yields the reverse effect. The minima observed on the intensity versus crystal-temperature curves are shifted to higher temperature with the inclusion of an increasing number of phonon events. The curve shape cannot be fitted by the usual Debye-Waller relation, a result in agreement with experimental results. However, the calculated intensities are in many cases greater than the measured ones. This can be due to the deficiencies of the chosen potential interaction or to an increase of anharmonic effects in the surface plane with respect to bulk anharmonicity.

I. INTRODUCTION

In the scattering of a particle by a solid or by the surface of a solid the intensities of the diffracted peaks are a decreasing function of the crystal temperature. For the case of neutrons or x-ray photon scattering, the evolution of the intensities with this parameter is well known and characterized by a so-called Debye-Waller factor. Due to a short-range-potential interaction, this evolution is obtained theoretically within the Born approximation.

For the scattering of neutral atoms or molecules by surfaces, the interaction potential is not very strongly localized on scattering centers as in the preceding case. The potential is periodic on a perfectly ordered surface and its thermal fluctuations are closely related to the thermal agitation of the crystal atoms. Therefore the Born approximation could not give good values of the intensities, and the T matrix must be calculated more exactly.

We have recently reported a new and a simple method which allows one to obtain an exact- T -matrix integral equation, the solution of which gives the T -matrix elements for the different diffracted beams^{1,2} and allows one to calculate exactly the cross section of inelastic events.

This method has been applied to the case of scattering by a flat surface, and the intensity of the specular peak as a function of the crystal temperature has been obtained. However, as the T -matrix equation is solved by an itera-

tive process the calculation thus far has been limited to the effect of one-¹⁻³ and two-phonon⁴ virtual exchange yielded by the second-, third-, and fourth-order expansion.

The results indicate clearly that the events involving three, four, etc. virtual phonons are not negligible even at medium crystal temperature. Thus, it appears necessary to include these events in order to recover the complete evolution of the scattered elastic intensity. The number of terms (or diagrams) which contribute to the T -matrix element of a process with n virtual-phonon exchange increases more rapidly than an exponential of n . Therefore, it is practically impossible to calculate their contribution term by term.

However, it is possible to construct a procedure which yields resummation of certain classes of the different contributions, starting with the matrix elements of the one- and two-phonon virtual exchange. This resummation procedure and the calculated specular intensity including many-phonon processes are presented in this paper.

In Sec. II the method giving the exact- T -matrix equation and the results concerning the one- and two-phonon processes which are necessary in order to build the resummation procedure are briefly recalled. The resummation is presented in Sec. III. The calculated intensities for the scattering of He, H₂, and Ne by the flat (100) face of copper are given in Sec. IV, and the results obtained are discussed in the last section.

II. T-MATRIX EQUATION: ONE- AND TWO-PHONON EXCHANGE

Levi and Suhl⁵ have shown that the diffracted peak intensities are proportional to the square modulus of the T -matrix element averaged over all crystal phonon states $\langle\langle T \rangle\rangle$. These quantities are solutions of the following T -matrix equation:¹

$$\begin{aligned} \langle\langle T \rangle\rangle = & \langle\langle V(\mathbf{R}, z, u) - U(z) \rangle\rangle \\ & - \frac{i}{\hbar} \int_0^\infty \langle\langle [V(\mathbf{R}, z, u(t)) - U(z)] \\ & \times \exp[i(c + i\varepsilon)t/\hbar] T \rangle\rangle dt, \quad (1) \end{aligned}$$

where $V(\mathbf{R}, z, u)$ is the interaction potential in which, as usual, \mathbf{R} and z label, respectively, the parallel and normal

components to the surface of vector space, and $U(z)$ is a distorted potential. u is an operator which depicts the potential thermal agitation, and $u(t)$ is the same operator taken in the interaction picture. $c = E_i - H_0$ where E_i is the particle incident energy and H_0 the distorted Hamiltonian

$$H_0 = -\frac{\hbar^2}{2m} \nabla^2 + U(z). \quad (2)$$

It contains the incident particle mass m .

In this work, we restrict ourselves to the study of the thermal attenuation of the specular peak yielded in the scattering by a flat surface. Putting

$$V(\mathbf{R}, z, u) - U(z) = v(z, u), \quad (3)$$

the integral equation is solved by iteration and the perturbation expansion is given by

$$\begin{aligned} \langle\langle {}_i T_i \rangle\rangle = & \langle\langle v u \rangle\rangle - \frac{i}{\hbar} \int_0^\infty dt \langle\langle v(u(t)) \exp[(ic - \varepsilon)t/\hbar] v(u) \rangle\rangle \\ & + \left[-\frac{i}{\hbar} \right]^2 \int_0^\infty dt_1 \int_0^\infty dt_2 \langle\langle v(u(t_1 + t_2)) \exp[(ic - \varepsilon)t_2/\hbar] v(u(t_1)) \exp[(ic - \varepsilon)t_1/\hbar] v(u) \rangle\rangle \\ & + \left[-\frac{i}{\hbar} \right]^3 \int_0^\infty dt_1 \int_0^\infty dt_2 \int_0^\infty dt_3 \langle\langle v(u(t_1 + t_2 + t_3)) \exp[(ic - \varepsilon)t_3/\hbar] v(u(t_1 + t_2)) \\ & \times \exp[(ic - \varepsilon)t_2/\hbar] v(u(t_1)) \exp[(ic - \varepsilon)t_1/\hbar] v(u) \rangle\rangle + \dots \quad (4) \end{aligned}$$

The introduction of projectors built with the eigenstates of H_0 , in the thermal average brackets, leads to c values which depend only on particle coordinates. Then the thermal average can be carried out, and after that the integration over t variables can be carried out. In this way, all order of expansion can be calculated exactly.

Following the above argument, the specular intensity is given by

$$I = \left| 1 - \frac{i\pi}{4p_i} {}_i F_i \right|^2, \quad (5)$$

where ${}_i F_i$ is the dimensionless $\langle\langle {}_i T_i \rangle\rangle$ matrix element. With the help of the inverse energy factor $A^2 = 2m/\hbar\chi^2$ we define the following dimensionless quantities.

matrix element	$\langle\langle {}_i T_i \rangle\rangle \rightarrow {}_i F_i = 4A^2 \langle\langle {}_i T_i \rangle\rangle$
frequency	$\omega \rightarrow \Omega = A^2 \hbar \omega$
energy:	
continuum state	$e_q \rightarrow q^2 = A^2 e_q$
bound state	$e_b \rightarrow \Omega_b = A^2 e_b $
time	$t \rightarrow \tau = \frac{t}{\hbar A^2}$

2χ is the damping coefficient of the repulsive part of the distorted potential. In this way, q_i is the dimensionless normal component of the incident wave vector k_i , namely, k_i^2/χ .

Owing to the lack of *ab initio* potential calculations, including the crystal atom thermal motion, we are led to represent the neutral particle surface interaction by a model potential. We choose the soft potential

$$V = D \{ \exp[-2\chi(z - u) - 2\chi^2 \langle\langle u^2 \rangle\rangle] - A(z) \}, \quad (6)$$

where u is the operator which describes the thermal displacement of the repulsive potential part normal to the surface. The attractive part is stationary with respect to thermal agitation.

For such a model potential the incident particle can gain or lose energy, but its component of momentum parallel to the surface is conserved. Because of this, the description of the physical reality is not complete. However, it can give realistic calculated intensity as discussed in detail in Ref. 4. This is mainly due to the fact that matrix elements of the potential decay rapidly for large phonon exchange. They act as a cutoff limiting phonon exchange largely to those of low frequencies, which are also those having low parallel momentum. Therefore the exchange of parallel momentum can be small.

Taking $U(z)$ equal to the thermal average of the potential, $v(u)$ is equal to

$$v(u) = D \exp(-2\chi z) [\exp(2\chi u - 2\chi^2 \langle\langle u^2 \rangle\rangle) - 1], \quad (7)$$

and the first-order term in the perturbation expansion (4) is equal to zero.

We examine now the shape of the different matrix elements yielded by the T -matrix expansion. For a given order of expansion p , one will see that the $\langle\langle {}_i T_i^{(p)} \rangle\rangle$ matrix element is a sum of terms, each of them involving a virtual exchange of n phonons:

$$\langle\langle {}_i T_i^{(p)} \rangle\rangle = \sum_{n=n_m}^{\infty} \langle\langle {}_i T_i^{(p,n)} \rangle\rangle .$$

$$\langle\langle {}_i T_i^{(2)} \rangle\rangle = \frac{-i}{\hbar} D^2 \left\langle e^{i\mathbf{K}_i \cdot \mathbf{R}} \phi_i \left| \int_0^{\infty} dt \exp(-2\chi z) \exp[(ic - \varepsilon)t/\hbar] [W(t,0) - 1] \exp(-2\chi z) \right| \phi_i e^{i\mathbf{K}_i \cdot \mathbf{R}} \right\rangle$$

with $|\mathbf{K}_i| = k_i \sin \theta_i$, k_i the incident wave vector, and θ_i the incident angle. ϕ_i is the eigenfunction ϕ_q of H_0 for $q = q_i$, and

$$W(t,0) = \exp[4\chi^2 \langle\langle u(t)u \rangle\rangle] .$$

The correlation function is given by

$$\langle\langle u(t)u \rangle\rangle = \frac{\hbar}{2M} \int_{-\omega_m}^{+\omega_m} \frac{\rho(\omega)}{\omega} \langle\langle n(\omega) \rangle\rangle \exp(i\omega t) dt , \quad (8)$$

where $\langle\langle n(\omega) \rangle\rangle$ is the Bose-Einstein factor, $\rho(\omega)$ the spectral density of u , and M the mass of a crystal atom.

In order to perform the t integration, $W(t,0)$ is expanded in powers of the correlation function. The different matrix elements $\langle\langle {}_i T_i^{(2,n)} \rangle\rangle$ can be easily calculated. For $n=1$ corresponding to the first term $4\chi^2 \langle\langle u(t)u \rangle\rangle$, one gets in dimensionless quantities

$${}_i F_i^{(2,1)} = 4(AD)^2 \left[\int_0^{\infty} q_i f_q G^{(2,1)}(c_q, T) q f_{q_i} dq + \sum_b q_i l_b G^{(2,1)}(c_b, T) b l_{q_i} \right] ,$$

with

$$G^{(2,1)} \left\{ \begin{matrix} (c_q, T) \\ (c_b, T) \end{matrix} \right\} = 4 \frac{m}{M} \int_{-\Omega_m}^{+\Omega_m} \frac{\rho(\Omega)}{\Omega} \langle\langle n(\Omega) \rangle\rangle \times d\Omega / \left[\left\{ \begin{matrix} c_q \\ c_b \end{matrix} \right\} + \Omega + i\varepsilon \right] ,$$

$$\langle\langle {}_i T_i^{(3)} \rangle\rangle = \left[\frac{-i}{\hbar} \right]^2 D^3 \left\langle e^{i\mathbf{K}_i \cdot \mathbf{R}} \phi_i \left| \int_0^{\infty} dt_1 \int_0^{\infty} dt_2 \exp(-2\chi z) \exp[(ic - \varepsilon)t_2/\hbar] \exp(-2\chi z) \right. \right. \\ \left. \left. \times \exp[(ic - \varepsilon)t_1/\hbar] \exp(-2\chi z) W(t_2, t_1) \right| e^{-i\mathbf{K}_i \cdot \mathbf{R}} \phi_i \right\rangle ,$$

with

$$W(t_2, t_1) = [W(t_2, 0) - 1][W(t_1, 0) - 1] \\ + [W(t_2, 0)W(t_1, 0) - 1][W(t_1 + t_2, 0) - 1] .$$

As in the case $p=2$, we expand the different W functions in powers of the correlation function. The contribution of

Due to the choice of the distorted potential, the minimum value of n , n_m is equal to $p/2$ or $(p+1)/2$ for p even or odd, respectively. This statement will be justified by examination of the different orders of expansion. As this has been done up to $p=4$ in Ref. 4, we give in the following a brief account of the analysis.

For $p=2$, after performing the thermal average one gets

$c_q = q_i^2 - q^2$, $c_b = q_i^2 + \Omega_b$. T is the crystal temperature and ${}_q f_{q_i}$ and ${}_b l_{q_i}$, respectively, the matrix element $\langle \phi_q | \exp(-2\chi z) | \phi_{q_i} \rangle$ and $\langle \phi_b | \exp(-2\chi z) | \phi_{q_i} \rangle$. The diagrammatic representation of ${}_i F_i^{(2,1)}$ is given in Fig. 1(a). The diagram is composed of two vertices which represent the f or l matrix element, located at the end of the bubble which account for the $G^{(2,1)}$ function. This last quantity contains a dressed propagator (c_q or $c_b + \Omega + i\varepsilon$). Therefore the diagram supposes an integration over the frequency Ω (bubble) and an integration over continuum state and a summation over bound states (vertices).

The matrix element $\langle\langle {}_i T_i^{(2,n)} \rangle\rangle$ coming from the n th power of the correlation function is similar to the preceding one. The $G^{(2,n)}$ function contains a dressed propagator (c_q or $c_b + \sum_{\gamma=1}^n \Omega_{\gamma} + i\varepsilon$)⁻¹, and consequently n integrations over the Ω_{γ} variables with the product of n factors $\rho(\Omega_{\gamma})/\Omega_{\gamma} \langle\langle n(\Omega_{\gamma}) \rangle\rangle$. $\langle\langle {}_i T_i^{(2,n)} \rangle\rangle$ is therefore proportional to $(1/n!)(m/M)^n$. Due to this factor and then n integrations, one can expect that the $\langle\langle {}_i T_i^{(2,n)} \rangle\rangle$ values will be negligible compared to $\langle\langle {}_i T_i^{(2,1)} \rangle\rangle$ value. This has been confirmed by numerical calculation. For all the systems considered in Ref. 4 (He-, Ne-, H₂-Cu) the $\langle\langle {}_i T_i^{(2,2)} \rangle\rangle$ values are negligible compared to $\langle\langle {}_i T_i^{(2,1)} \rangle\rangle$ and also compared to $\langle\langle {}_i T_i^{(p,2)} \rangle\rangle$ for $p=3$ and 4; that is to say, compared to the other matrix element giving the totality of the two-phonon events. The diagram for $\langle\langle {}_i T_i^{(2,2)} \rangle\rangle$ is given in Fig. 1(b).

For $p=3$, just after the thermal average evaluation one gets

the lower order term to the t_1 and t_2 integration is composed of three terms:

$$\exp[i(\omega_1 t_1 + \omega_2 t_2)] , \\ \exp\{i[\omega_1 t_1 + (\omega_1 + \omega_2) t_2]\} , \\ \exp\{i[\omega_2 t_2 + (\omega_2 + \omega_1) t_1]\} .$$

The integrations yield two types of propagators with one or two phonons, each of them located between two $\exp(-2\chi z)$ factors.

The calculation is carried out by introducing two appropriate projectors which transform the factors $\exp(-2\chi z)$ into matrix elements f , l , or j with $j = \langle \phi_b | \exp(-2\chi z) | \phi_b \rangle$. Clearly these terms depict virtual two-phonon processes. The corresponding diagrams

$$\langle\langle {}_i F_i^{(3,2)} \rangle\rangle = 4(A^2 D)^3 \int_0^\infty \int_0^\infty q_r f_q q f_r [G^{(3,2)}(c_q, c_r, T) + G^{(3,2)}(c_r, c_q, T)]_r f_{q_i} dq dr ,$$

with

$$G^{(3,2)}(c_2, c_1, T) = 4 \frac{m}{M} \int_{-\Omega_m}^{+\Omega_m} \frac{\rho(\Omega)}{\Omega} \langle\langle n(\Omega) \rangle\rangle \frac{d\Omega}{c_2 + \Omega + i\epsilon} \\ \times G^{(2,1)}(c_1 + \Omega, T) .$$

As expected, there are two integrations over Ω variables and the matrix element value is proportional to $(m/M)^2$.

For $p=4$, the same procedure as above yields three matrix elements depicting a two-phonon virtual exchange. Their diagrams are given in Fig. 1(d) in the order "bubble," "exchange," and "direct."

Their matrix elements are given in Ref. 4. It is, however, interesting to write here the one relevant for the bubble diagram. One has

$${}_i F_i^{(4,2)} = \frac{1}{4} \left[\int_0^\infty dq F^{(2,1)}(q_i, q) \frac{1}{c_q + i\epsilon} F^{(2,1)}(q, q_i) \right. \\ \left. + \sum_b F^{(2,1)}(q_i, b) \frac{1}{c_b} F^{(2,1)}(b, q_i) \right] ,$$

where $F^{(2,1)}(q, q_i)$ and $F^{(2,1)}(b, q_i)$ are, respectively, the matrix elements of the second order and one phonon process, between initial state q_i and final state q or b . Between two $F^{(2,1)}$ quantities there is a free propagator. Then it is evident that this kind of diagram leads to T -matrix elements which can be obtained by the linkage of two simpler ones, through a free propagator.

To higher order, terms in the expansion in powers of the correlation function for $p=3$ or 4 correspond to the matrix elements $\langle\langle {}_i T_i^{(3,n)} \rangle\rangle$ and $\langle\langle {}_i T_i^{(4,n)} \rangle\rangle$ with $n > 2$. One could write their expression using the above procedure, but this leads to lengthy calculations. It is more convenient to draw first the different diagrams which compose the (p, n) process, and then for each diagram write its T -matrix element. The rules which allow one to achieve correctly this procedure are given in the general case where p is greater than 4, as follows.

For $p > 4$, all the $\langle\langle {}_i T_i^{(p,n)} \rangle\rangle$ matrix elements which have been calculated ($p \leq 4$) can be represented by a diagram in which there is no vertex that is not connected to a phonon line. This is a consequence of our choice of a distorted potential which is the thermal average of the total interaction potential. All elastic matrix elements vanish in the averaging process.

This rule is equivalently to saying that there are never two consecutive free propagators. Consequently, the minimum number n_m of phonons involved in a p -order

are given in Fig. 1(c).

For illustration and completeness, we write the matrix element corresponding to the sum of the two symmetric diagrams. It is composed of four terms describing the transition via continuum-continuum states, via continuum and bound states and vice versa, and via bound-bound states. We illustrate for the first case. One gets

term of expansion is $p/2$ or $(p+1)/2$ for p even or odd, respectively. Always, with this rule, one can draw recursively the different diagrams corresponding to a (p, n) given process. Let us consider the set of $(6, 3)$ diagrams. There are six vertices and three phonon lines. If we connect two vertices with one phonon line, there remain four free vertices which one can connect with the remaining two phonon lines. The number of different possibilities is equivalent to that of a $(4, 3)$ diagram. Thus, for each phonon line, we have three $(6, 3)$ diagrams and on the whole 27 possibilities. One should, in fact, eliminate the duplication, and finally there remain 15 different diagrams (Fig. 2).

For p large, for example, greater than 8, this procedure is also length and not practicable except if it can be achieved on a computer. However, it can be sufficient to know the total number of diagrams belonging to the set (p, n) . This number is given by the expression⁶

$$N^{(p,n)} = \sum_{i=0}^p \frac{c_n^i (-1)^i (p-i)^n (p-i-1)^n}{2^n (n!)}. \quad (9)$$

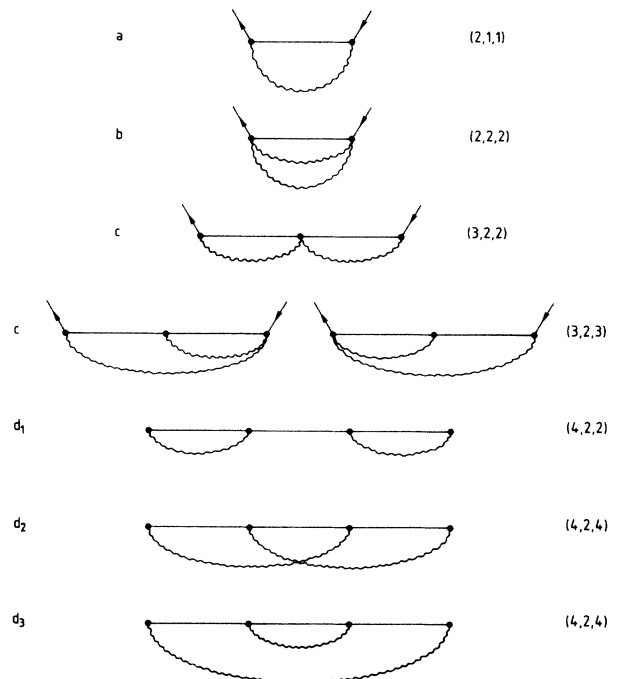


FIG. 1. Diagram representation of (a) one- and (b)–(d) two-phonon virtual process. d_1 , d_2 , and d_3 are called the bubble, exchange, and direct diagrams, respectively.

In fact, $N^{(p,n)}$ corresponds to the exact value for $n = n_m$. Otherwise ($n > n_m$) the number calculated in this way may be equal or less than the actual value. Table I gives the $N^{(p,n)}$ values and those determined by the diagram construction procedure. One sees that for a given order of perturbation p the number of diagrams increases very rapidly with the number n of virtual phonons exchanged.

A given diagram (p,n) contains p vertices, $p-1$ propagators, and n phonon lines, each of them connecting two vertices. In the associated T -matrix element, to each propagator corresponds univocally an integration over a given τ variable. Each phonon line yields a factor

$$\exp[i\Omega(\tau_r + \tau_{r+1} + \dots + \tau_R)]$$

where R is equal to the number of propagators comprised between the two vertices. In order to perform the τ integration the different $\exp(i\Omega_\gamma\tau)$ at fixed τ value are collected and this gives for each τ variable an integrand

$$\exp[(ic - \varepsilon)\tau] \exp\left[i\tau \sum_{\gamma=1}^s \Omega_\gamma\right],$$

where s is equal to the number of phonon lines, which on the diagram are drawn in front of the propagator associated to the τ variable. The integration yields a Green operator,

$$\left[c + \sum_{\gamma=1}^s \Omega_\gamma + i\varepsilon\right]^{-1}.$$

Since each phonon line is associated with an (n -fold) integration over $\Omega_1, \Omega_2, \dots, \Omega_n$, the $G^{(p,n,S)}$ function is given by

$$G^{(p,n,S)} = \left[\frac{4m}{M}\right]^n \int_{-\Omega_m}^{+\Omega_m} \dots \int_{-\Omega_m}^{+\Omega_m} \left[\prod_{\gamma=1}^n d\Omega_\gamma \frac{\rho(\Omega_\gamma)}{\Omega_\gamma} \langle\langle n(\Omega_\gamma) \rangle\rangle \right] \prod_{q=1}^{p-1} 1 / \left[c_q + \sum_{\gamma=1}^{s_q} \Omega_\gamma + i\varepsilon \right] \quad (10)$$

with

$$S = \sum_{q=1}^{p-1} s_q.$$

The complete expression of the T -matrix element is now obtained by the introduction of $p-1$ projectors. This produces the appearance of $2^{(p-1)}$ terms depicting the different possible ways of transition through continuum and bound states, to which are associated the matrix elements f , l , or j (total number p). At each f there corresponds an integration over continuum states and to each l or j there corresponds a summation over bound states. In this way the T -matrix element associated with a given diagram can be written explicitly. For instance, the term yielding only transitions via continuum states is given by a $[(p-1)$ -fold] integration over q_1, q_2, \dots, q_{p-1} as follows:

$$F^{(p,n,s)} = 4(A^2D)^p \int_0^\infty \dots \int_0^\infty p_i f_{q_1} \left[\prod_{r=1}^{p-2} q_r f_{q_{r+1}} dq_r \right]_{q_{p-1} f_{p_i}} dq_{p-1} G^{(p,n,s)}(C_1, C_2, \dots, C_{p-1}, T). \quad (11)$$

From this point a diagram will be labeled by a triplet of integers (p,n,S) where p is the order in perturbation expansion, n is the number of virtual phonon exchanged, and S is the sum over propagators of the number of phonon lines drawn in front of each of them.

III. RESUMMATION PROCEDURE

Let us consider a diagram which contains a free propagator G_e^+ . Each vertex of this operator being connected to a phonon line, the diagram can be decomposed into two

TABLE I. Number of diagrams for a given order of perturbation expansion p and a given number of virtual phonons exchanged n . $N^{(p,n)}$ is the number given by Eq. (9). N_e is the number given by the recursion procedure and n_m is the minimum number of virtual phonons at a given p .

p	n	n_m	$N^{(p,n)}$	N_e
2	1	1	1	1
3	2	2	3	3
3	3		8	8
4	2	2	3	3
4	3		19	22
5	3	3	30	30
5	4		180	
5	5		530	
6	3	3	15	15
6	4		352	
6	5		2260	
7	4	4	315	
7	5		5040	
7	6		35 312	
8	4	4	105	105
8	5		6090	
8	6		86 005	
9	5	5	3780	
9	6		126 000	
9	7		1 714 230	
10	5	5	945	
10	6		109 462	
10	7		2 876 580	

subdiagrams limited by the free propagator. If their matrix elements are known, the total matrix element can be easily calculated as in the case of the bubble diagram analyzed in the preceding section. Let ${}_i F_i^{(p_1, n_1, S_1)}$ and ${}_i F_i^{(p_2, n_2, S_2)}$ be the two submatrix elements. The connection by the G_e^+ operator yields a new diagram following the relation

$$(p_1, n_1, S_1) G_e^+ (p_2, n_2, S_2) = (p_1 + p_2, n_1 + n_2, S_1 + S_2) \quad (12)$$

and the new matrix element is given by the equation

$${}_i F_i^{(p_1+p_2, n_1+n_2, S_1+S_2)} = \frac{1}{4} \left[\int_0^\infty \frac{{}_{p_i} F_q^{(p_1, n_1, S_1)} {}_q F_{p_i}^{(p_2, n_2, S_2)}}{p_i^2 - q^2 + i\epsilon} + \sum_b \frac{{}_{p_i} F_b^{(p_1, n_1, S_1)} {}_b F_{p_i}^{(p_2, n_2, S_2)}}{p_i^2 + \Omega_b^2} \right].$$

On the other hand, one can define an operator g which has the effect of connecting directly two different subdiagrams. This yields a new diagram following the relation:

$$\text{Diagram 1} \quad g \quad \text{Diagram 2} = \text{Diagram 3}, \tag{13}$$

$$(p_1, n_1, S_1)g(p_2, n_2, S_2) = (p_1 + p_2 - 1, n_1 + n_2, S_1 + S_2),$$

and the new matrix element is given by

$${}_i F_i^{(p_1+p_2-1, n_1+n_2, S_1+S_2)} = \int_0^\infty {}_{p_i} J_q^{(p_1, n_1, S_1)} {}_q F_{p_i}^{(p_2, n_2, S_2)} dq + \sum_b {}_{p_i} J_b^{(p_1, n_1, S_1)} {}_b F_{p_i}^{(p_2, n_2, S_2)},$$

where ${}_{p_i} J_q^{(p_1, n_1, S_1)}$ is the matrix element ${}_{p_i} F_q^{(p_1, n_1, S_1)}$, except that the first matrix element f, l on the right, and the corresponding integration or summation has been removed.

Let us now define a new T -matrix element, say T_R , which is a solution of the equation

$$T_R = \Lambda + \Gamma(g + G_e^+)T_R, \tag{14}$$

where Λ and Γ are a sum of known matrix elements of low-order (p, n) diagrams.

The iteration of this equation generates new matrix elements corresponding to diagrams deduced from that contained in Λ and Γ by direct touching connections and by connection through a free propagator. One has

$$\begin{aligned} T_R^{(1)} &= \Lambda, \\ T_R^{(2)} &= \Gamma + \Gamma(g + G_e^+)\Lambda, \\ T_R^{(3)} &= \Lambda + \Gamma(g + G_e^+)\Lambda + \Gamma(g + G_e^+)\Gamma(g + G_e^+)\Lambda. \end{aligned}$$

The successive iterations give the sum of T -matrix elements of a defined subset of diagrams (p, n, S) obtained by application of relations (12) and (13). The actual set of diagrams is more or less well reproduced, depending upon the diagrams matrix elements introduced in Λ and Γ .

Those of Fig. 1 have been previously calculated.⁴ Thus we take for λ and Γ the sum

$$\begin{aligned} \lambda &= \text{Diagram 1} + \text{Diagram 2} + \text{Diagram 3} + \text{Diagram 4} \\ &+ \text{Diagram 5} + \text{Diagram 6}, \\ \Gamma &= \text{Diagram 7} + \text{Diagram 8} + X_3(t) \left[\text{Diagram 9} \quad \text{Diagram 10} \right] \\ &+ X_4(t) \left[\text{Diagram 11} \quad \text{Diagram 12} \right], \end{aligned}$$

where $X_3(t)$ and $X_4(t)$ are numbers suitably chosen varying from one iteration step (labeled by the integer t) to another. The second iteration yields the missing two-phonon diagrams $(3,2,2)$ and $(4,2,2)$ but also generates diagrams of $(3,3,S)$ to $(6,3,S)$ and of $(4,4,S)$ to $(8,4,S)$. Generally speaking, the lowest- and highest-order diagrams

generated at iteration t are, respectively, $(t+1, t, t)$ coming from the direct connection of $(2,1,1)$ diagrams, and $(4t, 2t, 4t)$ coming from connection of the $(4,2,4)$ diagrams through free propagators. In particular, the iteration process does not generate diagrams including n phonon events beyond the n th iteration step.

The set of $(6,3,S)$, $(5,3,S)$, and $(4,3,S)$ diagrams are reproduced in Figs. 2, 3, and 4, respectively. The diagrams which are generated by the iteration process are indicated. Some of them appear independently of X_3 and X_4 values, some others are their matrix elements multiplied by these numbers. It is clear that the choice $X_3(2)=X_4(2)=1$ does not take into account the contribution of many diagrams. Thus we have to choose these two numbers in such a way that the total matrix element given by the iteration is equivalent to the actual total matrix element. This can be achieved if we have an equivalence rule between two diagrams.

Let us consider the set of diagram (p,n,S) for given p and n . Expression (11) shows that their T -matrix elements are given by the same number of integrations or summations over continuum or bound states and that the integrand differs only by the $G^{(p,n,S)}$ function. This last quantity [expression (10)] is given by the same number of Ω integrations in which the products of $p-1$ Green operators vary from one diagram to another. For a given Green operator, the number s_q of phonons involved can vary from 0 (free propagator) to n . It yields, after the difference Ω integrations, a contribution which decreases as s_q increases. Thus the efficiency of a diagram is certainly linked to the sum of the different s_q value called S above. We make the assumption that the T -matrix element is inversely proportional to S , a rule useful for comparing two diagrams of the same p and n values. This equivalence rule has been tested with the $(3,2)$ and $(4,2)$ diagrams.⁴ For all the systems studied (He-Cu,Ne-Cu,H₂-Cu) at different incident particle energies and angles this rule holds if we do not consider the more or less large dispersion around the exact value. Thus it will be used for the determination of the appropriate $X_3(t)$ and $X_4(t)$ values.

Another result has been previously noticed⁴ which is relevant for this determination. It has been demonstrated that the importance of diagrams $(4,2,S)$ is greater than those of $(3,2,S)$, which are themselves greater than the $(2,2,2)$, whatever the S value may be. Furthermore, this has been proved for any p value ($n=\text{const}$),⁶ where if one neglects the bound state transitions and the principal value in the integration over continuum states one can show that the diagrams having the most important contribution to the intensity are those of order $p=2n$.

As the $(2n+2, n+1, S)$ diagrams generated by the iteration are multiplied by $X_4(t=n)$, this value will be determined using the equivalence rule within the order $p=2n+2$. After that, the $X_3(t=n)$ number will be fixed by applying the equivalence inside the set of diagrams $(2n+1, n+1, S)$.

Let us consider the set $(6,3,S)$. Taking the reference $S=5$, there are 12 diagrams which are not generated by the iteration process regardless of the X_3 and X_4 values. They are equivalent to

$$2 \frac{5}{5} + 4 \frac{5}{7} + 6 \frac{5}{9} = 8.19 \text{ diagrams ,}$$

where $S=5$ or 0.6825 for each diagram. They should be accounted for by $2 \cdot X_4(2)$ diagrams, $S=5$. Therefore

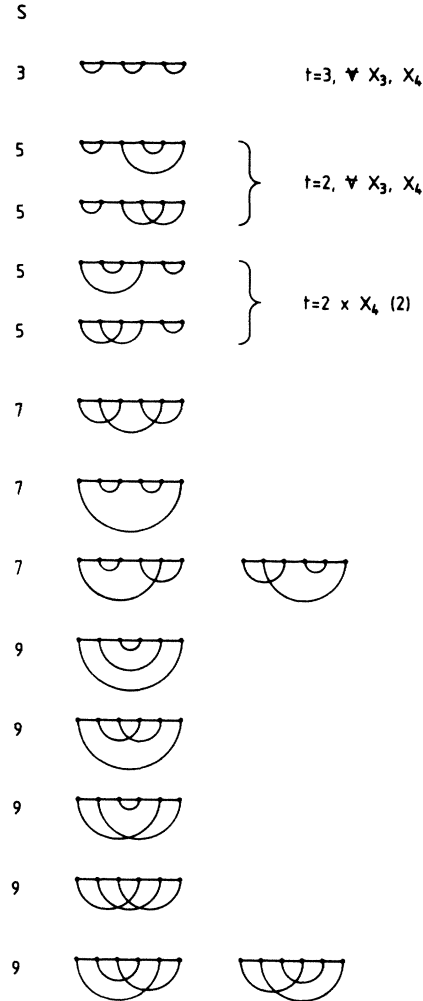


FIG. 2. Diagrammatic representation of the set $(6,3,S)$. The diagrams generated by the iteration procedure are indicated (iteration step t). Some are independent of X_3 and X_4 values, others have their matrix element multiplied by these numbers.

$$X_4(2) = \frac{8.19}{2} = 4.095 .$$

We take $X_4(2)=X_4(2)=4$.

The same procedure applied to the set $(5,3,S)$ (see Fig. 3) gives the following equation for the reference $S=4$:

$$2 \frac{4}{4} + 2 \frac{4}{5} + 8 \frac{4}{6} + 6 \frac{4}{7} + 6 \frac{4}{8} = 2 \frac{4}{4} X_3(2) + 2 \frac{4}{5} X_4(2) ,$$

which gives with $X_4(2)=4$, $X_3(2)=4.48$.

The left-hand side means that the 24 diagrams are equivalent to 15.36 diagrams with $S=4$ or 0.64 for each diagram.

To complete this analysis of the three-phonon virtual exchange, it remains to examine the sets of $(3,3,S)$ and $(4,3,S)$. In the former, there are two diagrams $(3,3,3)$ automatically generated by the iteration process and five others equivalent to 3.45 diagrams $(3,3,3)$ which are not

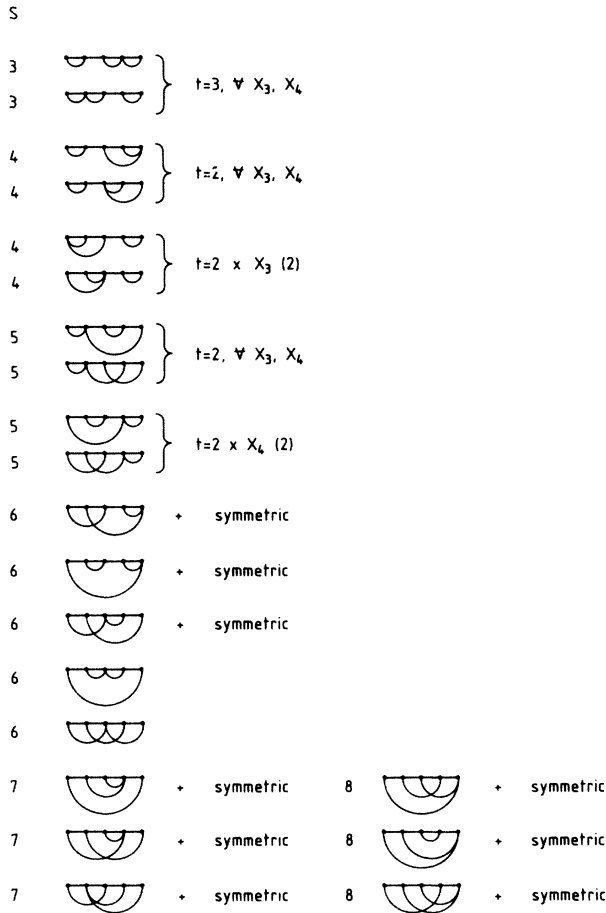


FIG. 3. Same as Fig. 2, but for the set (5,3,S).

taken into account. For the latter, the diagrams not included in the iteration are equivalent to (see Fig. 4)

$$2\frac{4}{4} + 7\frac{4}{5} + 6\frac{4}{6} + 2\frac{4}{7} = 12.74 \text{ diagrams } (4,3,4),$$

with $X_3(2)=4.48$, approximately nine diagrams are generated. In order to compensate for these deficiencies without modifying strongly the equivalence in the (5,3,S) set, we ascribe to $X_3(2)$ the value 5.

The different (8,4,S) diagrams have been enumerated. There are 105 diagrams of which 3 are automatically included in the iterations 3 or 4. If one excludes the last ones, they are equivalent to 56 diagrams (8,4,6), and each diagram contributes an average of 0.55 diagrams (8,4,6). The iteration provides $2[X_4(3)+X_4(2)]$ (8,4,6) and $4X_4(2)$ (8,4,8). Writing the equivalence relation, one finds $X_4(3)=18$.

The enumeration of the diagrams (7,4,S) is a lengthy operation as there are at least 315 diagrams (Table I). However, one can ascribe to $X_3(3)$ a realistic value. For that, we notice in the preceding analysis that one diagrams is, respectively, equivalent to 0.6825, 0.64, and 0.55 of diagrams (6,3,5), (5,3,4), and (8,4,6). Thus the number

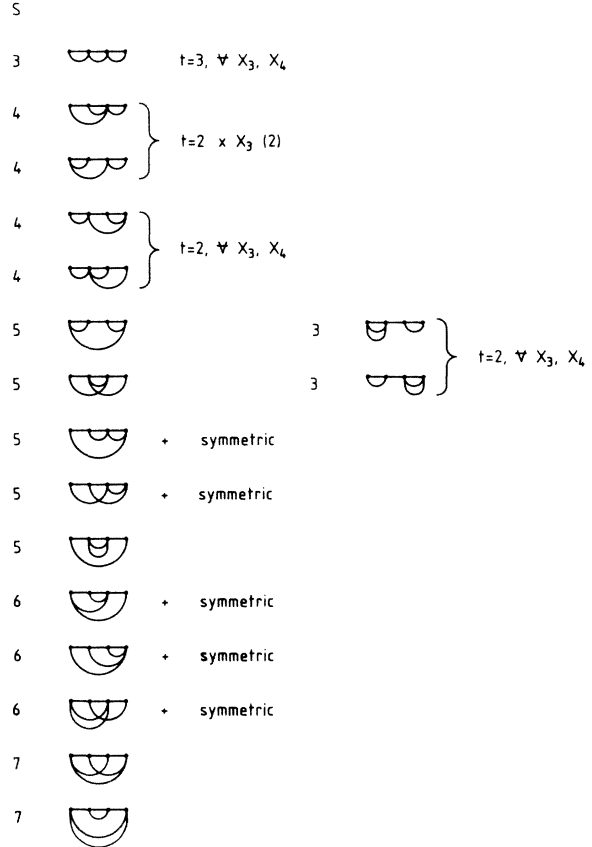


FIG. 4. Same as Fig. 2, but for the set (4,3,S).

of equivalent diagrams for the set (7,4,S) is taken equal to $315 \times 0.515 \approx 162$ with reference to $S=5$. The iteration generates

$$t = 2, 4[X_3(2) + X_4(2)] (7,4,7), \quad 4X_{4(2)} (7,4,8)$$

$$t = 3, 2 + 2X_3(2) + 2X_3(3) (7,4,5),$$

$$4 + 4X_4(2) + 4X_4(3) (7,4,6).$$

Writing the equivalence relation one gets $X_3(3)=19$.

The determination of $X_4(4)$ and $X_3(4)$ values by writing the equivalence relation, with the sets of diagrams (10,5,S) and (9,5,S), respectively, follows the same procedure as those used in the determination of $X_3(3)$. Taking each diagram equivalent to 0.5 of a (10,5,9) or (9,5,9) we get $X_4(4)=25$, $X_3(4)=0$.

As the order of iteration increases, it becomes more and more difficult to ascribe realistic values to the numbers $X(t)$. This is due to the rapidly increasing number of diagrams in the sets $(2n, n, S)$ and $(2n-1, n, S)$ which prevent their classification in subsets of given S values. Also, a small error in the first X numbers like $X_3(2)$ and $X_4(2)$ or $X_3(3)$ and $X_4(3)$ can be amplified by the successive iterations. Thus, it seems preferable to stop the iteration process at this point, that is to say, at iteration 4.

IV. RESULTS

Before performing numerical calculations, one should ascribe definite values to the potential parameters in such a way that the potential so defined leads to a good representation of the physical interaction. This has been the subject of a detailed discussion, particularly in Ref. 4. Here we keep the same potential representation and recall only its salient features.

The u operator is taken to be equal to the average displacement, normal to the surface, of four atoms belonging to the unit cell of a (100) copper face (a close-packed surface). The spectral density of u is then

$$\rho(\Omega) = \frac{1}{4}\rho_{11}^z(\Omega) + \frac{1}{2}\rho_{12}^z(\Omega) + \frac{1}{4}\rho_{13}^z(\Omega),$$

where the subscripts 12 and 13 label, respectively, the correlated spectral density between nearest- and next-nearest-neighbor atoms. The different ρ quantities have been previously calculated.⁷

The crystal anharmonicity is introduced through the quasiharmonic approximation. The maximum crystal frequency decreases as its temperature increases, and this variation is deduced from a nearest-neighbor potential calculation.⁸ The frequency values are in agreement with the corresponding measured quantities in neutron scattering experiments as discussed in Ref. 4. In this manner, the anharmonicity in the surface plane is taken to be that of the bulk crystal.

The shape of the potential attractive part $A(z)$ [Eq. (6)] is certainly a parameter which has a small influence on the calculated intensity. For convenience, $A(z)$ is taken equal to $2\exp(-\chi z)$ so that the distorted potential is of Morse shape. Consequently the thermal displacement of the potential repulsive part is equal to $2u$ or u , respectively, for values of the potential equal to zero or infinity. In order to recover a displacement equal to u in the range of small incident particle energy the u operator is divided by 2. Consequently, the spectral density is divided by 4.

The remaining parameters D and χ vary with the nature of the surface and of the incident particle. For a given particle, they are taken equal to those which fit the experimental data in an elastic diffraction experiment. They are listed in Table II.

The calculated results are presented in Figs. 5–13. The points represent the experimental data.^{12–14} They have been translated along the vertical axis by an amount equal to the experimental unitarity defect. One can see the results as follows: for He-Cu scattering, $E_i = 21$ meV, in Figs. 5–7; for He-Cu scattering, $E_i = 63$ meV, in Figs. 8–10; for H₂-Cu scattering, $E_i = 77$ meV, in Figs. 11 and

TABLE II. Parameter values for the potentials used in the calculation for the different incident particles.

Incident particle	D (meV)	χ_1 (Å)	Fit on	Ref.
He	6.35	1.05	(110),(113), (115),(117)	9
H ₂	21.6	0.97	(110),(115)	10
Ne	12.2	1.9	(110)	11

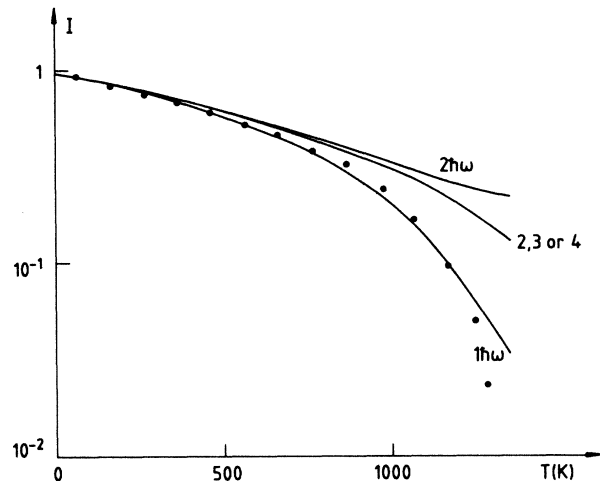


FIG. 5. Calculated intensities for helium-copper with $E_i = 21$ meV and $\theta_i = 73.5^\circ$. The curves labeled $1\hbar\omega$ and $2\hbar\omega$ are, respectively, the intensities given by the one-phonon and the one- plus two-phonon events. The resummed intensity curves are labeled by the iteration step number. Experimental data are from Ref. 12.

12; and for Ne-Cu scattering, $E_i = 63$ meV, in Fig. 13.

In each figure the intensities given by the one-phonon and the one- plus two-phonon processes are reported for comparison (see the curves labeled $1\hbar\omega$ and $2\hbar\omega$, respectively). The resummed intensities are represented by three superimposed or different curves and are labeled by the order of iteration: 2, 3, or 4.

V. DISCUSSION

The results yielded by this resummation procedure are obviously dependent upon the values ascribed to the numbers $X_3(t)$ and $X_4(t)$. Within the validity of the equivalence rule between diagrams having the same p and n orders, the $X_4(2)$, $X_3(2)$, and $X_4(3)$ numbers are determined accurately. On the contrary, the $X_3(3)$, $X_4(4)$, and $X_3(4)$ values determined in the same way are not so accu-

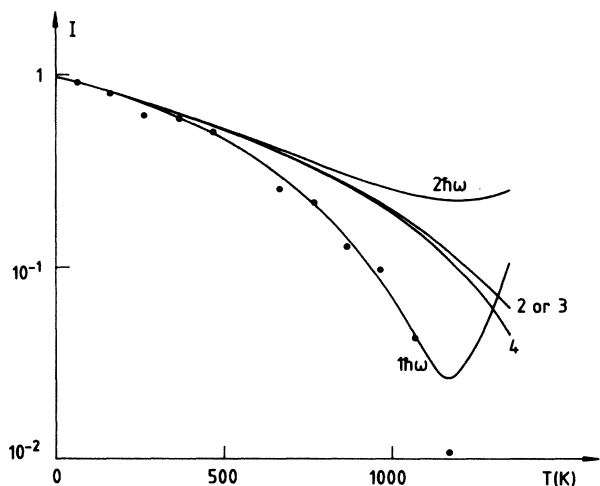


FIG. 6. Same as Fig. 5, but for $E_i = 21$ meV and $\theta_i = 55.5^\circ$.

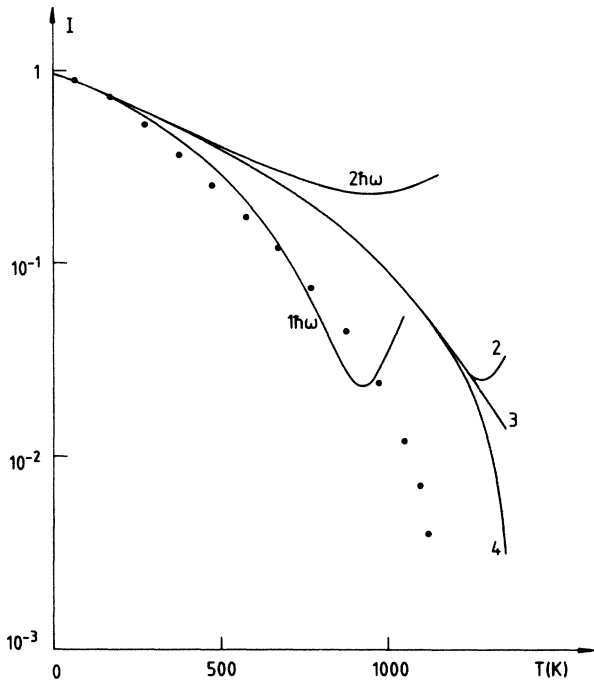


FIG. 7. Same as Fig. 5, but for $E_i=21$ meV and $\theta_i=31.8^\circ$.

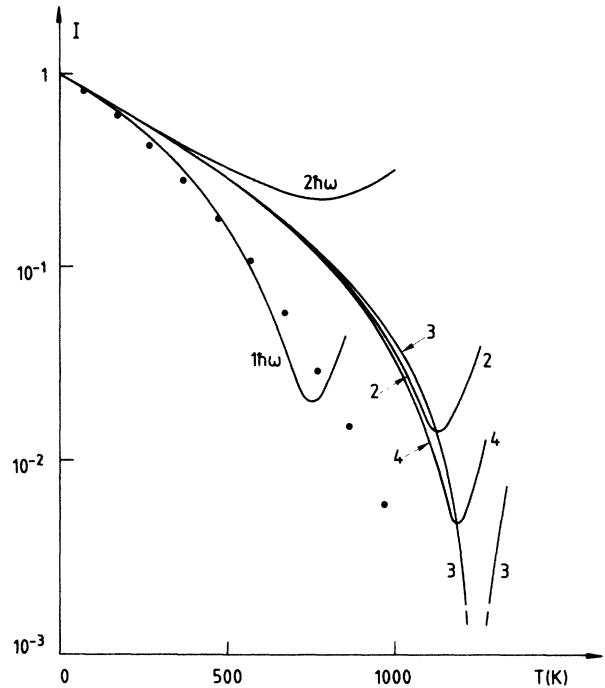


FIG. 9. Same as Fig. 5, but for $E_i=63$ meV and $\theta_i=51.5^\circ$.

rate, due to the difficulty of the enumeration of the difference diagrams belonging to the sets $(7,4,S)$, $(10,5,S)$, and $(9,5,S)$. It appears, then, necessary to perform the calculation with values for these three numbers differing somewhat from the chosen ones. Such calculations show that the intensities are not sensibly affected and that the calculation process remains stable. Thus the correctness of our choice is supported.

The introduction of the $(2,1,1)$, $(2,2,2)$, $(3,2,3)$, and

$(4,2,4)$ diagrams in the T_R -matrix equation leads to the appearance of diagrams of different p and n values in each iteration step. As a function of this integer, Table III gives their numbers calculated with the $X_3(t)$ and $X_4(t)$ values defined above. The two-phonon processes are correctly and completely included at iteration 2. But this iteration step generates also the near totality of the

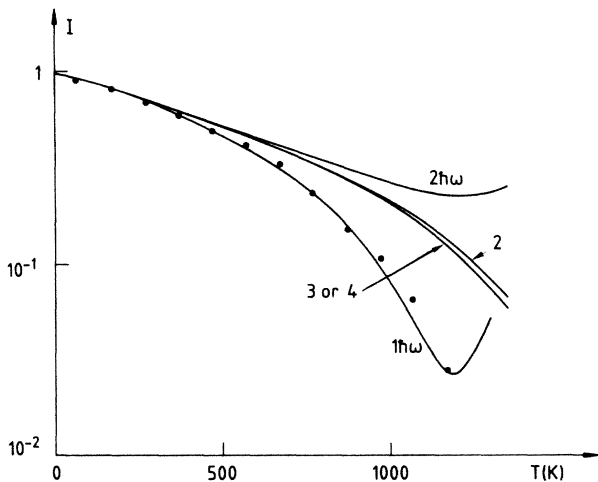


FIG. 8. Same as Fig. 5, but for $E_i=63$ meV and $\theta_i=71.6^\circ$.

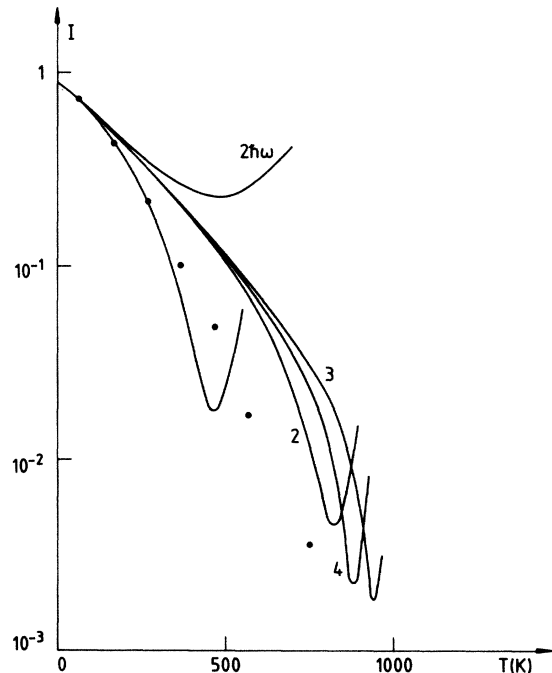


FIG. 10. Same as Fig. 5, but for $E_i=63$ meV and $\theta_i=19^\circ$.

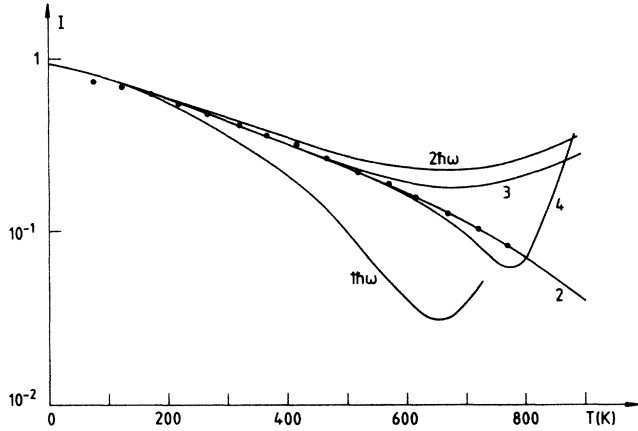


FIG. 11. Same as Fig. 5, but for molecular hydrogen on copper with $E_i=77$ meV and $\theta_i=75.5^\circ$. Experimental data are from Ref. 13.

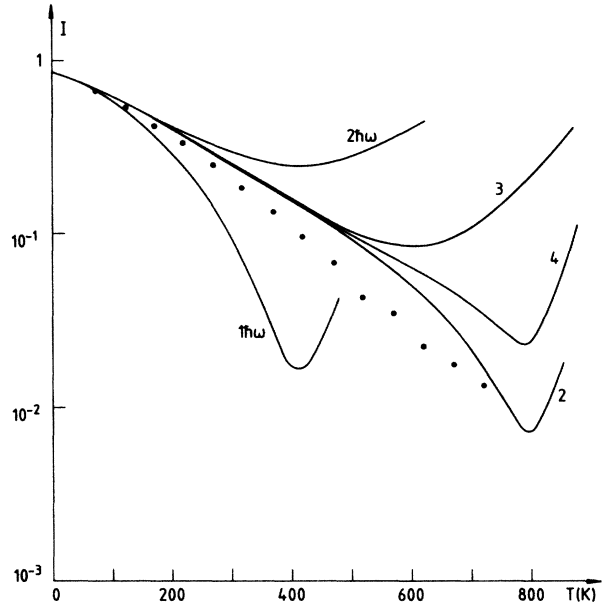


FIG. 12. Same as Fig. 11, but for $E_i=77$ meV, $\theta_i=31^\circ$.

three-phonon virtual exchange and approximately 30% of the (8,4,5) and (7,4,5) diagrams. At iteration 3, the four-phonon processes is almost complete and an important number of five- and six-phonon diagrams are generated. Generally speaking, and as noticed above, the n th step generates diagrams of $n, n+1, \dots, 2n$ phonon virtual exchange. This fact precludes the possibility of looking for a temperature at which the three-phonon, four-phonon, etc., processes become non-negligible. However, one can define a temperature T_M for which the multiphonon processes become as important compared to the one-plus two-phonon contributions. Table IV gives the T_M values which vary from one system to another in the expected way. In particular, the comparison between the scattering

of helium and the molecular hydrogen for the same incident particle energy and angle shows the influence of the well depth.

For all the systems and conditions studied here the resummed intensities are comprised between those given by the one- and one- plus two-phonon process. Moreover, the intensities of iteration 2 seem to be lower than those given by iteration 3, itself greater than those yielded by iteration 4. One can be tempted to say that an even number of phonon events increases the intensities, whereas an

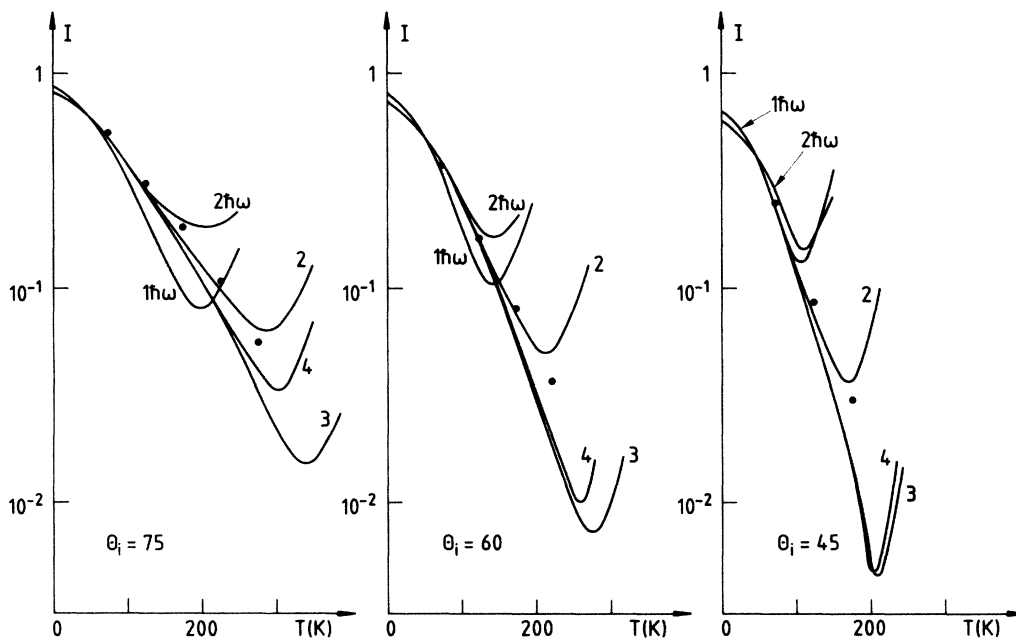


FIG. 13. Same as Fig. 5, but for neon on copper with $E_i=63$ meV, $\theta_i=75^\circ, 60^\circ, 45^\circ$. Experimental data are from Ref. 14.

TABLE III. Number of diagrams generated at each iteration step for each set (p, n, S) .

Diagram \ Iteration	2	3	4
(3,3,3)	2		
(3,4,S)			
(4,3,S)	14	1	
(4,4,S)	13	3	
(5,3,S)	22	2	
(5,4,S)	42	56	1
(5,5,S)		106	4
(6,3,S)	10	1	
(6,4,S)	66	149	3
(6,5,S)		771	62
(7,4,S)	52	142	3
(7,5,S)		2084	258
(7,6,S)		2702	1232
(8,4,S)	16	46	1
(8,5,S)		2640	442
(8,6,S)		6202	6096
(9,5,S)		1600	338
(9,6,S)		8440	15162
(9,7,S)			57478
(10,5,S)		376	96
(10,6,S)		6858	18836
(10,7,S)			161632

odd number yields the reverse effect. This particular behavior has been exhibited within the framework of energy shell approximations⁶ and the present calculation, which do not make this approximation seem to confirm this statement.

The intensity versus temperature curves exhibit a minimum except in the case of low energy exchange (He-Cu at $\theta_i = 73.5^\circ$). The minima are located at approximately the same temperature for the one-phonon and one-plus two-phonon processes, and this indicates that well before this temperature the higher order phonon events yield a non-negligible contribution to the calculated intensities. The resummed curves confirm this interpretation. They do not exhibit such a minima in Figs. 5–8, an indication that for these systems and conditions the order of virtual-phonon exchange included in the calculation is sufficient to describe the evolution of the intensities. On the contrary, minima appear on the resummed intensities on Figs. 9–13; that is, for systems and conditions in which the exchange of energy between the particle and crystal is the greatest. Its appearance indicates that the diagrams of larger numbers of phonon events could not be neglected in the calculation in the high-temperature range. However, the results obtained here are certainly valuable up to a temperature at least equal to those of the minima observed on the one-plus two-phonon events.

The measured and calculated intensities are in good agreement for the neon-copper system and for the molecular hydrogen-copper at incident angles of 75.5° (Figs. 13 and 11, respectively). However, in the former case, the

TABLE IV. Temperature at which the n th phonon process gives a non-negligible contribution to the calculated intensity. T_2 corresponds to $n=2$ and T_M is for $n \geq 3$.

	E_i	θ_i	T_2	T_M
He-Cu	21 meV	73.5	450	800
		55.5	300	600
		31.8	250	500
	63 meV	71.6	400	550
		51.5	180	350
		19	100	250
H ₂ -Cu	77 meV	75.5	150	300
		31	100	200
Ne-Cu	63 meV	$\forall \theta_i$	0	100–150

measured intensities are not very precise, particularly for the highest temperature, where the specular intensity emerges from a large diffuse foot. In the latter case the large incident angle excludes the possibility of an important exchange of energy, and the agreement is not convincing. This argument holds in the scattering of helium at 73.5° where disagreement is obvious. But in many cases, the measured intensities are lower than the resummed ones in the medium- and high-temperature range, and are rather well reproduced by the one-phonon process alone. This disagreement may be due to the deficiencies of the model of the potential and could be due to two effects.

(i) The thermal displacement of the potential repulsive part which has been related to the thermal displacement normal to the surface of four atoms belonging to the (100) unit cell. This certainly accounts for the main influence. However the contribution of atoms surrounding the unit cell and the parallel displacement to the surface of all atoms may not be negligible. This yields a slight increase of the u operator correlation function and, consequently, a decrease of the intensities, especially in the high-temperature range.

(ii) The exchange of parallel momentum in our potential model. As discussed in Ref. 4, this deficiency seems to be acceptable since the exchange of the virtual phonon proceeds mainly from the phonons of low frequencies; that is, with those having the smallest parallel momentum. However, this effect could be accounted for here in an arbitrary way, by a modification of the value $\alpha = \frac{1}{4}$, which multiplies the spectral density and which is chosen in order to recover the correct thermal displacement. The decrease of calculated intensities could be obtained in this way by an increase of α , the amount of which increase has been difficult to appreciate.

On the other hand, the observed disagreement could be due to an increase of anharmonic effects in the surface plane. The calculation takes account of anharmonicity but supposes that such effects are identical in the surface planes and in the bulk. If the nearest-neighbor potentials used to determine these effects quantitatively are modified in the first few surface planes, the surface anharmonicity could be different. To recover the measured intensities, it

would be necessary to increase the surface anharmonic effects. This variation is certainly in the expected direction.

VI. CONCLUSIONS

Starting with an exact procedure which gives the T -matrix elements for the one- plus two-virtual-phonon exchange, we have built a resummation procedure which includes multiphonon events. The adequacy of the calculated intensities thus depends only upon the chosen interaction and the method can be used to test the validity of a given potential.

The calculation has been performed in the case of a particle scattered by a flat surface. The potential which models the interaction is of a one-dimensional type and consequently precludes the exchange of parallel momentum. With a good representation of the phonon spectral density and anharmonic effects, the results compare very favorably with experimental data.

The evolution of the specular intensity with crystal temperature is definitely not represented by a usual

Debye-Waller factor. The three- and higher-order phonon processes become important at a crystal temperature which for copper is comprised between 100 and 800 K, depending upon the particle and the incident conditions (see Table IV). Furthermore, events involving more than five virtual phonons seem not to be negligible at high temperature. This high-temperature value varies from one system to another depending on the incident conditions, but could be estimated to be approximately equal to 200 K for neon and 650 K for the molecular hydrogen system. For helium its value depends strongly upon the incident energy and angle but roughly speaking is of the order of the copper melting point for incident energy of 21 meV. At an energy of 63 meV it could be as low as 800 K near normal incidence.

The results presented in this paper outline the importance of multiphonon processes in the scattering of atoms and molecules by surfaces. The agreement obtained with the available experimental data indicates that the most important contribution to energy exchange for these incident conditions is through phonon processes.

*Present address: Max-Planck-Institut für Festkörperforschung, Heisenbergstrasse 1, D-7000 Stuttgart 80, Federal Republic of Germany.

¹G. Armand and J. R. Manson, *Phys. Rev. Lett.* **53**, 1112 (1984).

²G. Armand and J. R. Manson, in *Dynamics on Surfaces*, edited by B. Pullman *et al.* (Reidel, Dordrecht, Holland, 1984), Vol. 17, p. 59.

³C. S. Jayanthi, G. Armand, and J. R. Manson, *Surf. Sci. Lett.* **154**, L247 (1985).

⁴G. Armand, J. R. Manson, and C. S. Jayanthi, *J. Phys. (Paris)* **47**, 1357 (1986).

⁵A. C. Levi and H. Suhl, *Surf. Sci.* **88**, 221 (1979).

⁶J. R. Manson and G. Armand, *Surf. Sci.* (to be published).

⁷G. Armand, *J. Phys. (Paris)* **38**, 989 (1977).

⁸C. S. Jayanthi, E. Tosatti, and A. Fasolini, *Phys. Rev. B* **31**, 470 (1985).

⁹D. Gorse, B. Salanon, F. Fabre, A. Kara, J. Perreau, G. Armand, and J. Lapujoulade, *Surf. Sci.* **147**, 611 (1984).

¹⁰J. Lapujoulade and J. Perreau, *Phys. Scr.* **T4**, 138 (1985).

¹¹B. Salanon, *J. Phys. (Paris)* **45**, 1373 (1984).

¹²D. Gorse and J. Lapujoulade, *Surf. Sci.* **162**, 847 (1985).

¹³J. Lapujoulade, Y. LeCrüer, M. Lefort, Y. Lejay, and E. Maurel, *Surf. Sci.* **103**, L85 (1981).

¹⁴J. Lapujoulade, Y. Lejay, and G. Armand, *Surf. Sci.* **95**, 107 (1980).